Space Shuttle Flutter as Affected by Wing-Body Aerodynamic Interaction

R. R. Chipman,* F. J. Rauch,† P. Shyprykevich,‡
Grumman Aerospace Corporation, Bethpage, N. Y.
and
R. W. Hess§
NASA Langley Research Center, Hampton, Va.

In the NASA Langley Research Center 26-in. transonic blowdown wind tunnel, flutter speeds were measured on 1/80th-scale semispan models of the orbiter wing, the complete Space Shuttle, and intermediate component combinations. Using the doublet lattice method combined with slender body theory to calculate unsteady aerodynamic forces, subsonic flutter speeds were computed for comparison. Aerodynamic interaction was found by test and analysis to raise the flutter speed in some configurations while lowering it in others. Although at Mach numbers less than 0.7, predicted speeds correlated to within 6% of those measured, rapid deterioration of the agreement occurred at higher subsonic Mach numbers, especially on the more complicated configurations. Additional analysis showed that aerodynamic forces arising from body flexibility potentially can have a large effect on flutter speed but that the current shuttle design is not so affected.

Nomenclature

b = reference semichord
c = local chord
D = matrix of influence coefficients relating downwash on all lifting surfaces to the pressures on them
ET = external hydrogen oxygen tank
F = matrix of influence coefficients relating downwash on all surface panels to the pressures on all lifting slender bodies
h = lifting element deformation normal to the body axis
k = reduced frequency $= \omega b/U_\infty$
M = Mach number
R_0 = local radius of a slender body
S = semispan of exposed wing
SRB = solid rocket booster
U_∞ = freestream speed
V_f = flutter speed
W = complex downwash $= U_\infty h' + i\omega h$
x = streamwise coordinate
y = spanwise coordinate
z = vertical coordinate
h' = angle of attack
ΔC_p = coefficient for the differential pressure on a lifting element
$\Delta C_{p,B}$ = coefficient of differential pressure acting on the projected area of a slender body
$\Delta C_{p,I}$ = coefficient of differential pressure on wing-body interference panels
$\Delta C_{p,w}$ = coefficient of differential pressure on a wing panel (or other lifting surface)
μ = mass density ratio
ρ = air density
ω = frequency
ω_r = reference frequency (wing first torsion, 449.5 Hz)
$()'$ = derivative in the freestream or x direction
$()''$ = second derivative in the freestream or x direction

Presented as Paper 74-363 at the AIAA/ASME/SAE 15th Structures, Structural Dynamics and Materials Conference, Las Vegas, Nevada, April 17-19, 1974; submitted April 11, 1974; revision received December 23, 1974. This work was performed under NASA contracts, NAS 1-10635-10 and NAS 1-10635-18, and Rockwell International Contract M3WX-MZ-483002.

Index categories: Aircraft Testing (including Component Wind Tunnel Testing); Spacecraft Configurational and Structural Design (including Loads); Aeroelasticity and Hydroelasticity.

*Senior Aeroelasticity Methods Engineer. Member AIAA.
†Senior Dynamics Engineer.
‡Senior Structural Mechanics Engineer. Member AIAA.
§Aerospace Research Engineer. Member AIAA.

Introduction

THE aerodynamic interaction of proximate components of a flight vehicle can give rise to aerodynamic forces sufficient to destabilize surfaces otherwise flutter-free within their flight envelope. On conventional aircraft, T-tail flutter[1,2] and wing-tail-fuselage flutter[3,4] are instances of this phenomenon. On early Space Shuttle designs, aerodynamic interaction between the orbiter wing and the wing of the proposed fly-back booster was found to affect flutter speed significantly.[5] For the present Space Shuttle, the proximity of the large, flexible bodies (orbiter fuselage, external tank and solid rocket boosters) to the orbiter wing (see Fig. 1) admits the possibility of an altered flutter boundary due to wing-body interaction.

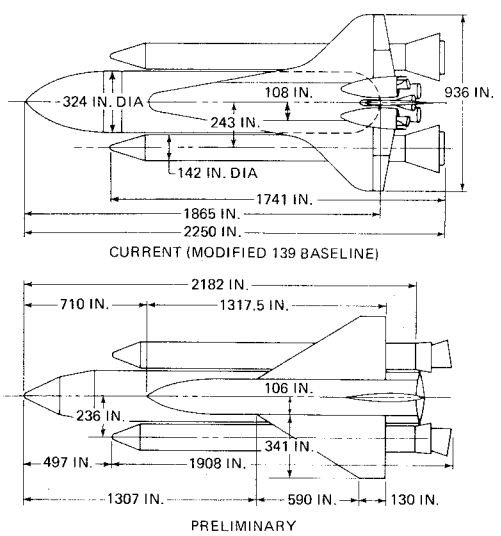

Fig. 1 Comparison of preliminary (GIIIA) and current design configurations.

The calculation of steady aerodynamic forces arising from the interaction between general bodies and lifting surfaces has been performed by Woodward[6] and Hess.[7] By extending the Woodward method to quasi-steady flow, Huntington[8] has shown that wing-body interaction effects can be substantial on vehicle gust response characteristics. The present paper uses a method developed by Rodden and Giesing[9] that combines thin-wing linear potential theory with slender body theory to determine unsteady aerodynamic forces subsonically. In this approach, axial doublets represent the bodies while panels of doublets are placed on the wing and on the body surfaces to account for interaction.

To determine the effect of aerodynamic interaction on the Space Shuttle and to evaluate the ability of the doublet-lattice method[9] to predict such effects, the present joint analytical and experimental study was conducted. Semispan models (1/80th-scale) of the Shuttle were tested for flutter transonically and the results of these tests were compared with subsonic flutter speeds calculated using the doublet lattice method. The models were constructed so that no structural coupling would exist between the various structural components. In this way, the effects of aerodynamic interaction would not be masked by structural interaction.

Since analysis performed on the preliminary design (Fig. 1) showed that aerodynamic forces arising from body flexibility did not appreciably alter the Space Shuttle flutter speed, the models of the bodies were designed to be rigid. Except for two configurations in which flexible solid rocket boosters attachments were used, only the wing was flexible. To provide an additional basis of comparison for the analysis, steady-state pressures were measured on the wing in the various configurations.

Test Apparatus

Models

Semispan models of the current Shuttle design shown in Fig. 1 were built for flutter testing. They consisted of rigid fairing replications of the orbiter half-fuselage, the half external-tank (ET), and the solid rocket booster (SRB) in proper proximity to a flexible orbiter wing. The wing is a double delta with an inner-panel leading-edge sweep of 79°, an outer-panel sweep of 45°, and an aspect ratio of 2.1. The wing model consisted of aluminum spanwise-tapered core plates with cutouts, designed to match the torsion-to-bending frequency ratio of the full-scale wing. Onto the core, balsa wood was affixed and shaved to a 12% maximum thickness airfoil shape representative of the Shuttle. Wing camber and twist were not replicated; the model section was made symmetrical. To eliminate structural coupling, the rigid geometrically scaled fairings representing the fuselage, ET, and SRB components were fastened rigidly to a splitter plate located at the mid-vehicle plane. This assembly is shown in Fig. 2. A second splitter plate was made that could be located at the wing root when the body fairings were removed to study flutter of the isolated wing end-plated at its root.

Two sets of flexible connectors were fabricated, each of which could be substituted for the rigid fasteners linking the SRB to the ET. With these flexures, SRB pitch and heave modes could be attained. One of the sets was designed such that the frequencies of these modes in model scale were equal to the nominal Shuttle design. With the second set, the frequencies were chosen to be closer to wing torsion so that the likelihood of interaction would be greater. Table 1 summarizes the frequencies of these and the primary wing modes.

For obtaining steady state pressure measurements, a rigid wing with 38 pressure taps was constructed. Provisions were made on the mounting plate to pitch each configuration either 0° or −3°. With pressure data from each of these two angles of attack, the primary effects of wing thickness could be removed by subtraction of the two pressure distributions.

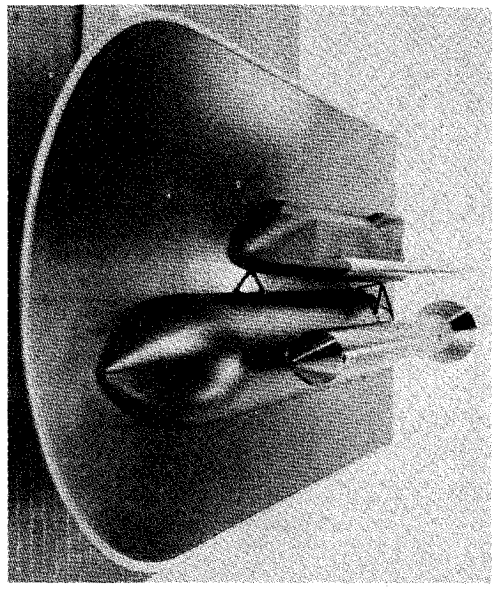

Fig. 2 Model assembly on splitter plate.

Instrumentation

Each flexible wing was instrumented with strain gauges which, through their response to bending and torsional motions, were used to detect the onset of flutter and to measure flutter frequency. Additional gauges were mounted on the SRB flexures to detect SRB excitation.

Wind Tunnel

Testing was conducted in the NASA Langley Research Center 26-in. Transonic Blowdown Wind Tunnel for a Mach number range of 0.6-1.4. High-speed movies were made of each flutter run.

Tunnel Tests

Flutter Tests

As shown in Table 2, flutter boundaries were determined for six configurations: the isolated wing end-plated at its root, the orbiter (wing and fuselage), the orbiter and external tank, the full-up Shuttle (orbiter, tank and SRB) with rigid in-

Table 1 Model frequencies

Mode	Frequency (hz)
Wing 1st bending	169.1
Wing 1st torsion	449.5
Wing 2nd bending	548.0
Wing 2nd torsion	912.1
Wing plate mode	1045.9
SRB Pitch	
Nominal flexure	124.0
Tuned flexure	222.0
SRB Heave	
Nominal flexure	242.9
Tuned flexure	438.0

Table 2 Model configurations

Configuration	Investigations performed[a]
1) Isolated wing	P and F
2) Orbiter	F
3) Orbiter / tank	P and F
4) Shuttle (rigid connection)	P and F
5) Shuttle (nominal flexure)	F
6) Shuttle (tuned flexure)	F

[a] P = pressure distribution (steady state); F = flutter boundary determination.

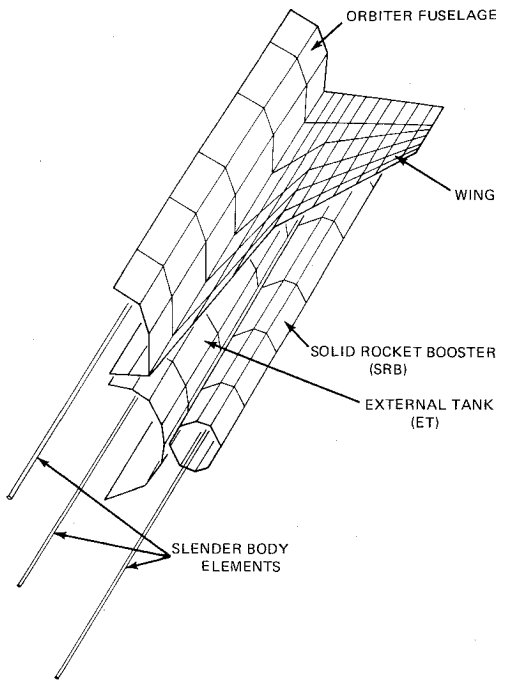

Fig. 3 Aerodynamic idealization of Space Shuttle.

terstage attachments, the full-up Shuttle with the nominal flexible attachments, and the full-up Shuttle with a second set of flexible attachments.

Pressure Tests

For each of the three configurations noted in Table 2, pressure measurements were made at $M=0.6$ and 0.8.

Theory

Using the doublet lattice method,[9] aerodynamic influence coefficients were calculated at various subsonic Mach numbers for the various configurations studied. As depicted in Fig. 3, the aerodynamic idealization consisted of panels having doublet lines at the panel 1/4-chords modeling the wing and the surfaces of the bodies in the vicinity of the wing—where interaction effects would be expected to be largest—and of axial doublets representing the bodies themselves.

The strengths of the axial doublets were determined separately, using slender body theory

$$\{\Delta C_{p,B}\} = 2\pi U_\infty \{R_0' h' + (R_0/2)h'' - (k^2/2b^2)R_0 h\} + 2\pi U_\infty (k/b)i\{R_0' h + R_0 h'\} \quad (1)$$

while the strengths of the body surface doublets were determined jointly with the wing doublets. To introduce coupling between the two solutions, the boundary conditions to be satisfied by panel doublets were modified by the downwash created by the axial doublets

$$\begin{Bmatrix} \Delta C_{p,w} \\ \Delta C_{p,I} \end{Bmatrix} = \begin{bmatrix} D_{w,w} & D_{w,I} \\ D_{I,w} & D_{I,I} \end{bmatrix}^{-1} \left\{ \begin{Bmatrix} W_w \\ W_I \end{Bmatrix} - \begin{bmatrix} F_{w,B} \\ F_{I,B} \end{bmatrix} \{\Delta C_{p,B}\} \right\} \quad (2)$$

Preliminary Analysis

Using a finite-element model that included the flexibilities of the wing, fuselage, external tank and SRB's, normal modes were calculated for a preliminary Space Shuttle design shown in Fig. 1. In calculating the unsteady pressures and, hence, the generalized aerodynamic forces required for the flutter analysis, all terms in Eqs. (1) and (2) were required. For comparison, a base case, containing no aerodynamic interaction, was run. For this case, Eq. (2) becomes

$$\{\Delta C_{p,w}\} = [D_{w,w}]^{-1}\{W_w\} \quad (3)$$

Flutter Model Analyses

Using measured modes, flutter solution were determined for the models tested. For configurations 1-4 of Table 2, the rigidity of the bodies causes the slender body pressure to vanish so that Eq. (2) becomes

$$\begin{Bmatrix} \Delta C_{p,w} \\ \Delta C_{p,I} \end{Bmatrix} = \begin{bmatrix} D_{w,w} & D_{w,I} \\ D_{I,w} & D_{I,I} \end{bmatrix}^{-1} \begin{Bmatrix} W_w \\ 0 \end{Bmatrix} \quad (4)$$

In configurations 5 and 6, the rigid SRB is allowed to heave and pitch and hence gives rise to slender-body pressures as calculated by Eq. (1). Since these modes have no curvature, however, the h'' term is zero.

Pressure Model Analyses

Steady state pressures were calculated to compare with the distributions measured on configurations 1, 3 and 4, at a constant angle of incidence to the flow. For this case, the slender body pressure reduces to

$$\{\Delta C_{p,B}\} = 2\pi U_\infty \{R_0' h_0'\} \quad (5)$$

Results

Preliminary Analysis

The results of these investigations are summarized in Table 3: The flutter speed of the critical instability is decreased 11% by interaction and of this only 3% is attributable to the aerodynamic effects of body flexibility. However, the flutter speed of a certain noncritical antisymmetric instability was decreased 30% with two-thirds of this change attributable to the aerodynamic effect of body flexibility. The modes associated with this instability include large lateral bending deflections of the fuselage brought about by its large flexibility—this design had non-load-carrying cargo doors in the orbiter midsection whereas the present design does not. This indicates the possibility that body flexibility could affect flutter speed significantly on future vehicles where soft midsections are employed, and shows that body flexibility should be included in the flutter analysis of such designs.

Model Flutter Results

Shown in Fig. 4 are the flutter speeds, flutter frequency indices and mass density ratio measured on the isolated wing. Also shown are the analytical results obtained at the test conditions. At Mach numbers below 0.9, the analytical flutter speed prediction is typically 6% conservative (using most unconservative test results), while the predicted flutter-frequencies are 5% low at worst. Hence, the correlation in this base-case is excellent.

Since the minimum measured V_f is only 4½% lower than the measured V_f at $M=0.68$, the wing can be said to have almost no transonic dip. Because the recovery in flutter speed is sharp, the level of the supersonic flutter speed was not ascertained. The flutter speed and flutter frequency indices

Table 3 Effect of body aerodynamics in preliminary analysis

Aerodynamic idealization	$V_{F\,\text{Shuttle}}/V_{F\,\text{Wing}}$	
	Symmetric	Antisymmetric
1) Body aerodynamics included	0.91	0.89
2) Body aerodynamics not included	0.94	0.92

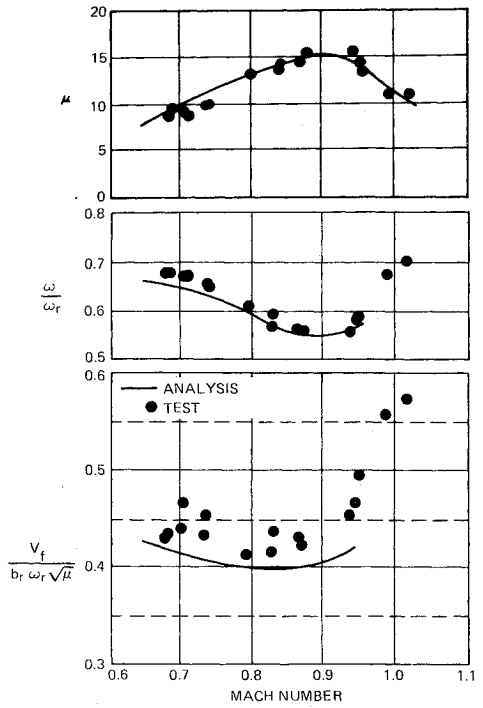

Fig. 4 Comparison of experimental and analytical flutter boundaries for isolated wing.

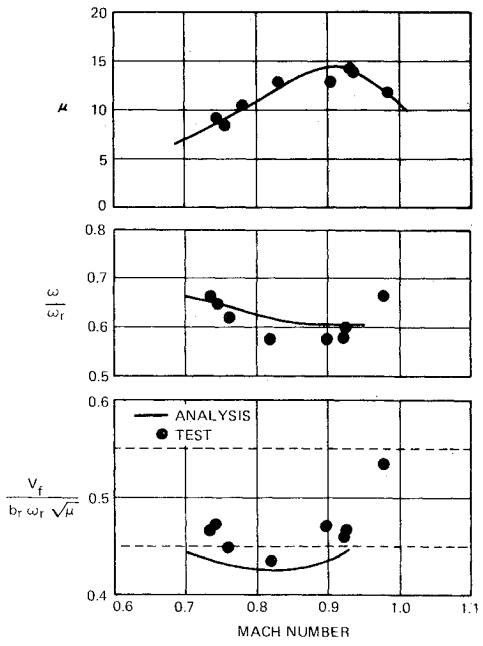

Fig. 5 Comparison of experimental and analytical flutter boundaries for orbiter.

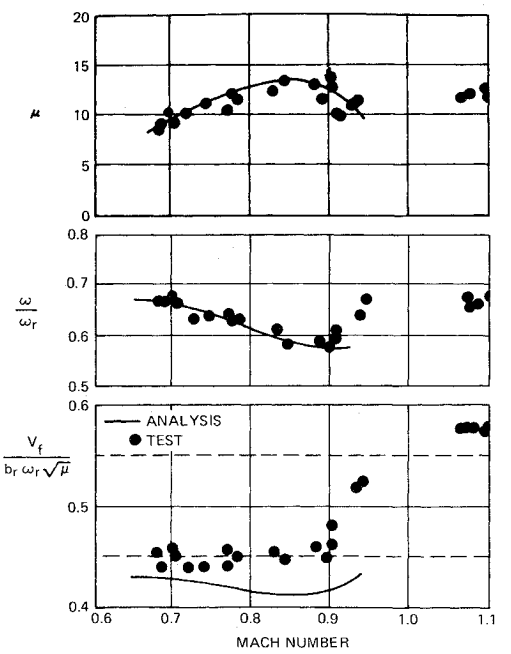

Fig. 6 Comparison of experimental and analytical flutter boundaries for orbiter/ET.

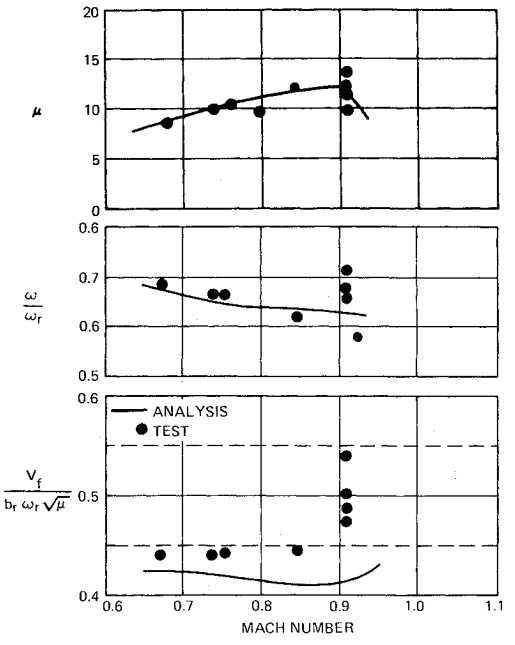

Fig. 7 Comparison of experimental and analytical flutter boundaries for Shuttle with rigid SRB attachments.

determined for the orbiter configuration are present in Fig. 5. Both experiment and analysis show that the subsonic flutter speed is higher than that of the wing alone. The accuracy of the predicted flutter speeds is still within 6% and that of frequencies is within 8%. Although the transonic dip of 7% is slightly more than occurs on the wing alone, it is still very shallow.

As can be seen in Fig. 6, agreement between test and analysis begins to deteriorate on the orbiter/tank configuration. Up to a Mach number of 0.8, the flutter speed correlate within 7%; but at $M=0.9$ the analysis is 11% conservative. On the full-up shuttle configuration with rigid SRB attachments, the Mach number at which correlation deteriorates is seen in Fig. 7 to shift lower. At $M=0.75$, the analytical flutter speeds is only 6½% low; but at $M=0.8$ and 0.85, the discrepancies are 9% and 13%, respectively. (Results for the flexible SRB attachments are presented later).

To compare the flutter boundary of the various configurations, it is necessary first to adjust the test data to a constant air density; for in the blowdown wind-tunnel different operating points in general correspond to different densities. This scaling was made by modifying the test V_f by the ratio of the analytical flutter speed at the desired density to that at the test point density. To minimize the amount of scaling to be made, the boundaries were adjusted to a typical tunnel density of three times that at sea level. Figure 8 shows the resulting test flutter boundaries.

At moderate subsonic Mach numbers ($M \leq 0.75$), the orbiter flutter speed is 7% higher than that of the wing, the orbiter/tank flutter speed is 3% higher than that of the wing, and the full-up Shuttle is only 1% higher. No appreciable

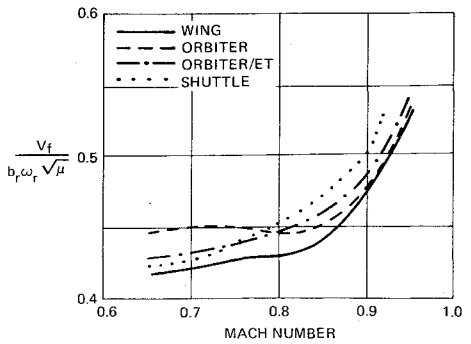

Fig. 8 Test flutter boundaries adjusted to a constant air density, $\rho = 3\rho_{S.L.}$

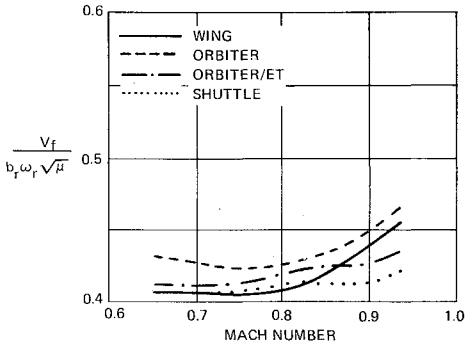

Fig. 9 Analytical flutter boundaries at a constant air density, $\rho = 3\rho_{S.L.}$.

transonic dip occurs on any configuration. Although all configurations show a sharp flutter speed increase as Mach one is approached, this recovery occurs at increasingly lower Mach numbers as the tank and the SRB are added to the vehicle. This trend causes the order of the flutter speeds to change at the high subsonic Mach numbers so that this order becomes: wing alone, lowest; orbiter higher; orbiter/tank, higher still; and complete Shuttle, highest. This shift in the recovery can probably be attributed to higher local Mach numbers in the vicinity of the tank and SRB when these components are added to the orbiter.

The analytical flutter boundaries at the same air density of three times that at sea level are shown in Fig. 9. At moderate subsonic Mach numbers, the trend is the same as revealed by experiment. As can be seen in Table 4, the predicted percentage differences in the flutter speeds of the various configurations are quite close to those measured at these Mach numbers. The transonic effects predicted, however, do not agree with experiment. The recovery is less and more gradual than experienced in the tests, and the presence of the tank and the SRB delay rather than speed the recovery. These failings of the analysis are not unexpected, since the theory assumes that Mach number is constant throughout the flowfield.

Table 4 Effect of aerodynamic interaction as obtained by analysis and test adjusted to a constant air density ratio of 3.0

Configuration	M	Vf/Vf of wing alone	
		Analysis	Test
Orbiter	0.7	1.05	1.07
	0.9	1.02	1.01
Orbiter/ET	0.7	1.02	1.03
	0.9	0.97	1.02
Shuttle	0.7	1.00	1.01
(Rigid coupling)	0.9	0.95	1.06
Shuttle	0.7	1.00	0.99
(Nominal flexures)	0.9	0.95	1.03
Shuttle	0.7	1.00	0.97
(Tuned flexures)	0.9	0.95	0.97

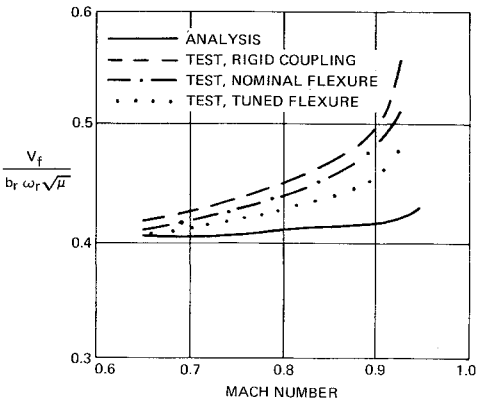

Fig. 10 Comparison of shuttle flutter speeds for various SRB attachment flexibilities at $\rho = 3\rho_{S.L.}$.

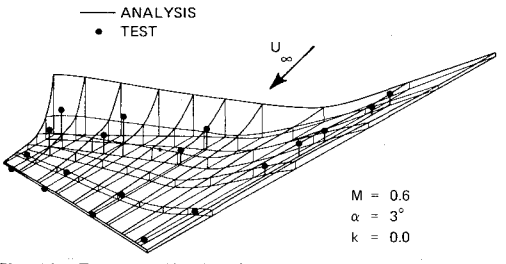

Fig. 11 Pressure distribution on isolated orbiter wing.

The adjusted flutter boundaries for the configurations with flexible SRB attachments are presented in Fig. 10. These flexibilities cause 2% and 4% decreases in the measured subsonic flutter speed relative to the rigid case, whereas the analytical flutter speed is unaffected. As seen in Table 1, the nominal SRB modes are close in frequency to the lowest wing mode; analysis shows that this couples with the second wing mode to produce the flutter instability, therefore, an effect by the SRB modes on the flutter speed is not unreasonable. For the tuned flexure, the frequencies of the SRB modes are close to the flutter frequency and the even greater effect on the flutter speed should be expected. The cause of the theory's failure to predict this effect is unknown. However, studies of the shuttle by Ericsson and Reding[10] have shown that flow separation occurs at the shoulder of the SRB nose. It is conceivable that when the SRB oscillates at frequencies close to the wing flutter frequency, shed vortices impinge upon the wing, causing significant deviations from the unsteady pressures expected from potential theory.

Pressure Correlation

For the isolated wing at $M = 0.6$, Fig. 11 shows the steady-state pressure distribution, ΔCp. Both the calculated and measured results are shown and the agreement is seen to be good. In Fig. 12, the inboard chord $(y/s = 0.1)$ of the distribution is shown by itself; in this plot the "spillover" lift from the outer panel of the double-delta wing can be seen to be adequately predicted.

For the three configurations for which pressures were measured, Figs. 12 and 13 give a comparison of the calculated and measured distributions at $Y/s = 0.1$ and 0.7 for $M = 0.6$. Tests and analysis show that replacing the root-chord reflection plane by the orbiter and tank lowers the pressure at the inboard leading edge of the wing; this effect diminishes outboard and aft. Agreement between test and analysis is good, with analysis overestimating the inboard pressure drop slightly. Similarly, the presence of the SRB lowers the pressure further at the inboard leading-edge and the amount of this decrease is again predicted reliably. At the inboard trailing edge, however, both theory and test show that the SRB causes a pressure increase, whereas outboard the SRB

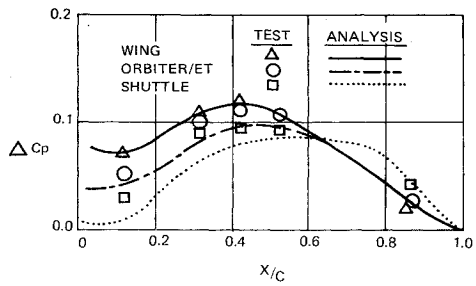

Fig. 12 Steady-state pressure distributions from test and analysis at $M=0.6$ ($Y/S=0.1$).

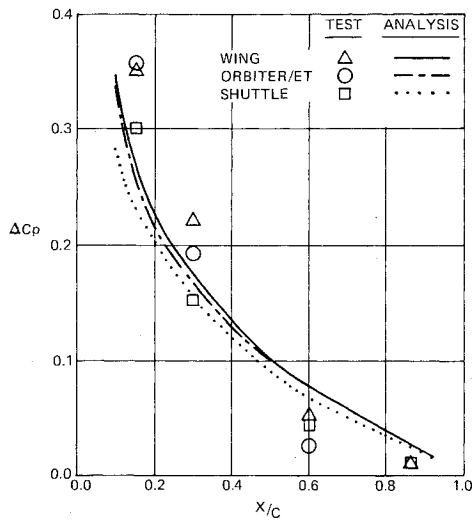

Fig. 13 Steady-state pressure distributions from test and analysis at $M=0.6$ ($Y/S=0.7$).

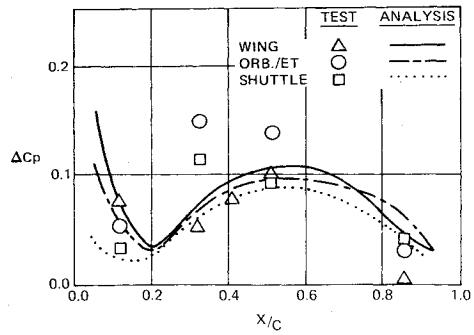

Fig. 14 Steady-state pressure distributions from test and analysis at $M=0.8$ ($Y/S=0.1$).

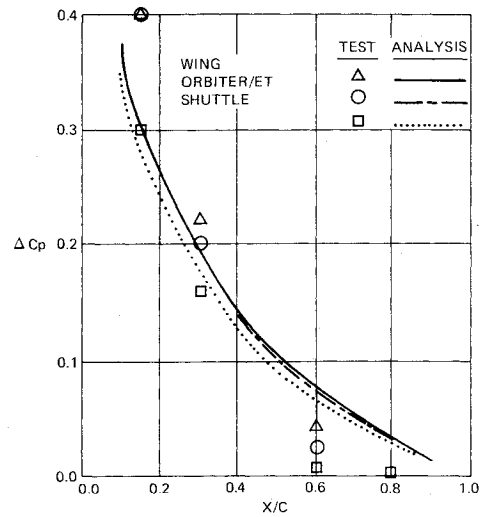

Fig. 15 Steady-state pressure distributions from test and analysis at $M=0.8$ ($Y/S=0.7$).

causes the pressure to drop. Overall, the correlation between test and analysis is good.

Figures 14 and 15 show a similar comparison of pressures at $M=0.8$. Generally, the analytical trends are the same as for $M=0.6$. The measured data, however, does not agree well with these trends. Outboard, the SRB decreases the pressure considerably more than predicted. Inboard, although the leading-edge pressures agree with theory, pressures on the remainder of the chord are higher for the more complex configurations that for the isolated wing—the reverse of the predicted trend. This lack of agreement is consistent with the flutter results and can probably be attributed to transonic flow phenomena not represented by the theory. There is also the possibility that the flowfield is being complicated by flow separation and shed vortices.

Conclusions

Aerodynamic interaction between the wing and bodies of a preliminary Space Shuttle design was found by analysis to cause an 11% change in flutter speed. The major portion of this effect was determined to be predictable without including the effects of body flexibility in the aerodynamics. However, an indication was found that body flexibility potentially could cause large changes in flutter speeds in other designs.

Tests and analyses of semispan models of the current design but using rigid bodies showed a slightly altered flutter boundary and indicated that analysis adequately predicted configurational trends at Mach numbers ≤ 0.7. Simulation of the flexibility in the SRB attachments caused a lowering of the stability boundary that was not predicted by the present analysis. Comparison of calculated and measured steady-state pressure distributions on various combinations of rigid Shuttle components indicated good correlation at $M=0.6$ but poor correlation for the wing-body configurations at $M=0.8$.

References

[1] Stahle, C. V., "Transonic Effects on T-Tail Flutter," RM-24, 1959, The Martin Company, Baltimore, Md.

[2] Stark, V. J. E., "Aerodynamic Forces on a Combination of a Wing and a Fin Oscillating in Subsonic Flow," SAAB TN54, Feb. 1964, Linkoping, Sweden.

[3] Sensberg, O. and Laschka, B., "Flutter Induced by Aerodynamic Interference between Wing and Tail," *Journal of Aircraft*, Vol. 7, July-Aug., 1970, pp. 319-324.

[4] Mykytow, W. J., Noll, T. E., Huttsell, L. J., and Shirk, M. H., "Investigations Concerning the Coupled Wing-Fuselage-Tail Flutter Phenomenon," *Journal of Aircraft*, Vol. 9, Jan. 1972, pp. 48-54.

[5] Chipman, R. R., Rauch, F. J., and Hess, R. W., "Flutter of Pairs of Aerodynamically Interfering Delta Wings," *Journal of Aircraft*, Vol. 10, Dec. 1973, pp. 728-734.

[6] Woodward, F. A., "Analysis and Design of Wing-Body Configurations at Subsonic and Supersonic Speeds," *Journal of Aircraft*, Vol. 5, Dec. 1968, pp. 528-534.

[7] Hess, J. L. and Smith, A. M. O., "Calculations of Non-Lifting Potential Flow About Arbitrary Three-Dimensional Bodies," DAC Report No. E.S. 40622, 1962, Douglas Aircraft Co., Los Angeles, Calif.

[8] Huntington, R. G., "Space Shuttle Response to Atmospheric Turbulence," AIAA Paper 73-310, Williamsburg, Va., 1973.

[9] Rodden, W. P., Giesing, J. P., and Kalman, T. P., "New Developments and Applications of the Subsonic Doublet-Lattice Method for Nonplanar Configurations," *AGARD Symposium on Unsteady Aerodynamics for Aeroelastic Analysis of Interfering Surfaces*, Paper No. 4, Tonsberg Oslofjorden, Norway, Nov. 1970.

[10] Ericsson, L. E. and Reding, J. P., "Unsteady Aerodynamic Analysis of Space Shuttle Vehicles," Rept. LMSC-D352320, Aug. 1973, Lockheed Missiles and Space Company, Sunnyvale, Calif.